Supporting information for: The Role of Momentum Partitioning in Covariance Ion Imaging Analysis

Tiffany Walmsley,[a,‡] Joseph W. McManus,[a,‡] Yoshiaki Kumagai,[b] Kiyonobu Nagaya,[c] James Harries,[d] Hiroshi Iwayama,[e,f] Michael N.R. Ashfold,[g] Mathew Britton,[h] Philip H. Bucksbaum,[i] Briony Downes-Ward,[j] Taran Driver,[h] David Heathcote,[a] Paul Hockett,[k] Andrew J. Howard,[i] Jason W. L. Lee,[l] Yusong Liu,[i] Edwin Kukk,[m] Dennis Milesevic,[a] Russell S. Minns,[g] Akinobu Niozu,[n] Johannes Niskanen,[m], Andrew J. Orr-Ewing[g], Shigeki Owada,[o,p] Patrick A. Robertson,[a] Daniel Rolles,[q] Artem Rudenko,[q] Kiyoshi Ueda,[r] James Unwin,[a] Claire Vallance,[a] Mark Brouard,[a] Michael Burt,[a,@] Felix Allum,[a,h,i,*] and Ruaridh Forbes[h,¶]

[a] *Chemistry Research Laboratory, Department of Chemistry, University of Oxford, Oxford OX1 3TA, United Kingdom*
[b] *Department of Applied Physics, Tokyo University of Agriculture and Technology, Tokyo, Japan*
[c] *Department of Physics, Kyoto University, Kyoto, 606-8502, Japan*
[d] *QST, SPring-8, Kouto 1-1-1, Sayo, Hyogo, 679-5148, Japan*
[e] *Institute for Molecular Science, Okazaki 444-8585, Japan*
[f] *Sokendai (The Graduate University for Advanced Studies), Okazaki 444-8585, Japan*
[g] *School of Chemistry, University of Bristol, Cantock's Close, Bristol BS8 1TS, U.K.*
[h] *Linac Coherent Light Source, SLAC National Accelerator Laboratory, Menlo Park, California 94025, USA*
[i] *PULSE Institute, SLAC National Accelerator Laboratory, 2575 Sand Hill Road, Menlo Park, CA 94025, USA*
[j] *School of Chemistry, University of Southampton, Highfield, Southampton SO17 1BJ, UK*
[k] *National Research Council of Canada, 100 Sussex Dr. Ottawa, ON K1A 0R6, Canada*
[l] *Deutsches Elektronen-Synchrotron (DESY), Notkestraße 85, 22607 Hamburg, Germany*
[m] *Department of Physics and Astronomy, University of Turku, Turku, FI-20014, Finland*
[n] *Graduate School of Advanced Science and Engineering, Hiroshima University, Higashi-Hiroshima 739-8526, Japan*
[o] *RIKEN SPring-8 Center, Sayo, Hyogo, 679-5148, Japan*
[p] *Japan Synchrotron Radiation Research Institute, Hyogo, Japan*
[q] *J. R. Macdonald Laboratory, Department of Physics, Kansas State University, Manhattan, KS, 66506, USA*
[r] *Department of Chemistry, Tohoku University, Sendai 980-8578, Japan*
‡ These authors contributed equally to this work
[@] michael.burt@chem.ox.ac.uk
[*] fallum@stanford.edu
[¶] ruforbes@slac.stanford.edu

1 Potential three-body sequential pathways of iodopropane

Due to the unique environment of each of the carbon atoms in 1-IP, there are many potential sequential mechanisms by which the parent dication can dissociate into three bodies. Figure S1 outlines the general fragmentation pathways of 1-IP that constitute a primary Coulomb explosion between two charged fragments, one of which is unstable and further dissociates by ejecting a neutral co-fragment. Loss of hydrogen(s) has been disregarded for simplicity. Covariance was only identified between ion pairs generated by the pathway highlighted in red.

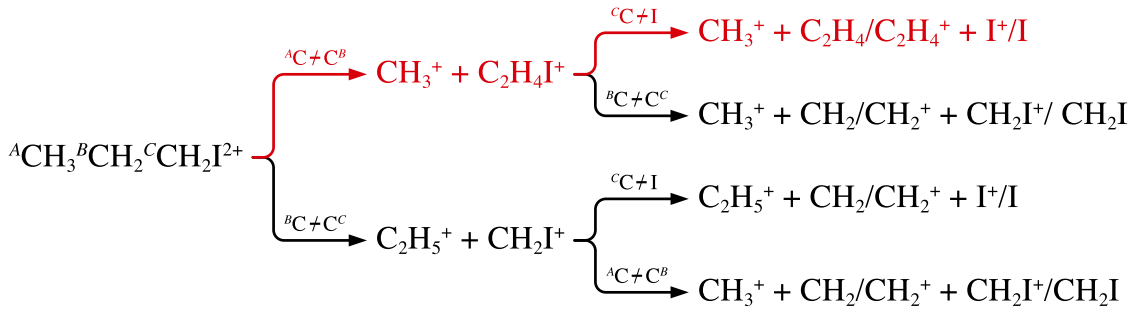

Figure S1: The potential three-body sequential dissociation channels of 1-IP^{2+} (disregarding C-H bond cleavage). Highlighted in red are channels that are observed to be statistically significant and are discussed in the main text.

2 Covariance analysis

To demonstrate in full how the procedure for isolating a specific sequential three-body breakup channel of a molecular dication works, we again consider the two-fold covariance between (I^+, $CH_3{}^+$) for 1-IP, and present the steps required to isolate channel (III):

$$\begin{aligned} C_3H_7I^{2+} &\rightarrow C_3H_7{}^+ + I^+, \\ C_3H_7{}^+ &\rightarrow CH_3{}^+ + C_2H_4. \end{aligned} \tag{III}$$

The raw covariance map is shown in Figure S2(a) which contains contributions from four identified fragmentation channels, as discussed in the main text.

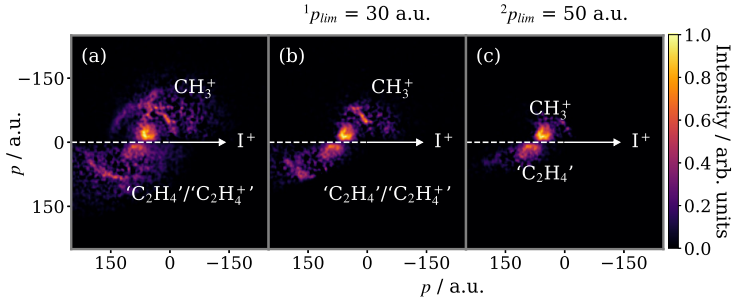

Figure S2: The successive steps used to isolate the feature corresponding to the sequential breakup of the parent dication, demonstrated for the Newton diagram constructed from the covariance of the (I^+ + CH_3^+) ion pair in 1-IP. (a) Raw covariance map; (b) imposing the condition $|\vec{p}_{CH_3^+}| = m_{CH_3}|\vec{p}_{I^+}|/m_{C_3H_7} \pm {}^1p_{lim}$; (c) imposing the second condition $|\vec{p}_{CH_3^+}| + |\vec{p}_{C_2H_4}| = |\vec{p}_{I^+}| \pm {}^2p_{lim}$.

To isolate channel (III), two constraints are applied to the ion momenta. The first is to impose the condition:

$$|\vec{p}_{CH_3^+}| = \frac{m_{CH_3}|\vec{p}_{I^+}|}{m_{C_3H_7}} \pm {}^1p_{lim}, \tag{1}$$

where $^1p_{lim}$ is a small quantity that accounts for ion pairs not exactly satisfying this relationship due to the impulse of the secondary dissociation. The effect this parameter has on the result of the covariance calculation is demonstrated in Figure S3. $^1p_{lim}$ is qualitatively chosen to be as small as possible, thereby removing the most signal from the other fragmentation channels, without visibly cropping the feature from the channel of interest in the Newton diagram. Here, a limit of 30 a.u. was found to give the best result. A unique $^1p_{lim}$ was found for each of the fragmentation pathways listed in panels (b) and (c) of Figure 4 in the main text.

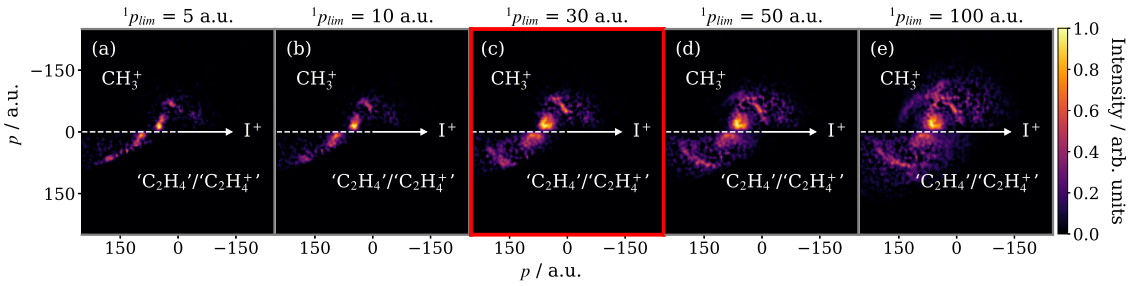

Figure S3: Newton diagrams constructed from the covariance of the (I^+ + CH_3^+) ion pair in 1-IP under the condition $|\vec{p}_{CH_3^+}| = m_{CH_3}|\vec{p}_{I^+}|/m_{C_3H_7} \pm {}^1p_{lim}$, as a function of $^1p_{lim}$. Outlined in red is the p_{lim} selected for this channel.

Some signal at a larger radius remains in Figure S2(b), which arises from channel (I), the sequential breakup of the trication. This is removed using a second condition that the magnitude of the sum of the momenta of secondary products must roughly equal the magnitude of the momentum of the primary product:

$$|\vec{p}_{CH_3^+}| + |\vec{p}_{C_2H_4}| = |\vec{p}_{I^+}| \pm {}^2p_{lim}. \tag{2}$$

Once again, a parameter ($^2p_{lim}$) is used to account for the impulse of the secondary dissociation. To obtain a value for this parameter, the raw covariance map is transformed into the COM frame of the secondary dissociation of $C_3H_7^{+/2+}$, shown in Figure S4. The momentum release of the secondary dissociation can then be determined from the extent of the central feature, as marked on the integrated radial distribution in the adjacent panel. The isolated signal for channel (III) after applying both of these momentum constraints is shown in Figure S2(c).

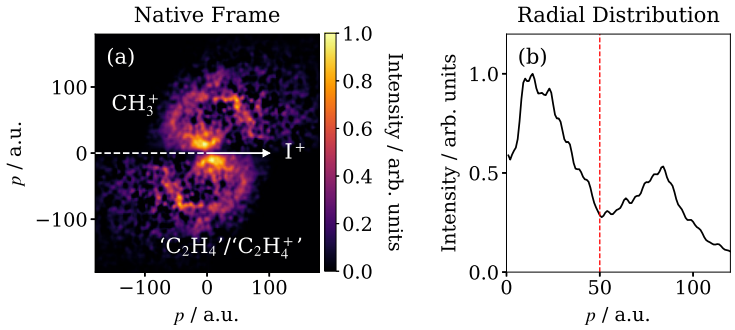

Figure S4: (a) Newton diagram for the breakup of 1-IP$^{2+/3+}$ into (I^+ + CH_3^+ + $C_2H_4/C_2H_4^+$) in the COM frame of the secondary dissociation $C_3H_7^{+/2+} \rightarrow CH_3^+ + C_2H_4/C_2H_4^+$. The radial momentum distribution of CH_3^+ in this frame is displayed in (b), with the selected $^2p_{lim}$ for this channel indicated by a dashed red line.

3 Momentum resolution of the spectrometer

The momentum resolution of the delay line hexanode detector was determined *via* a two-fold covariance analysis between I^+ and $C_3H_7^+$. Because these two fragment ions together constitute the original parent molecule, the sum of their momenta should exactly equal zero. The correlated momentum sum distribution for this pair of ions, plotted in Figure S5, is centered at zero but has a finite width. The uncertainty in the momentum resolution of the spectrometer was estimated from the standard deviation of a Gaussian fitting.

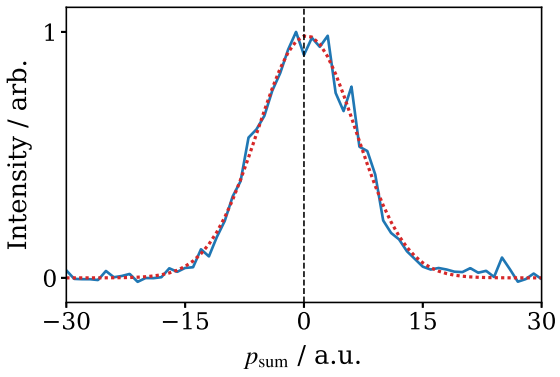

Figure S5: (*Blue*) Momentum sum distribution for the fragments of the two-body breakup of 2-IP^{2+} into (I^+ + $C_3H_7^+$). (*Red dotted*) A Gaussian fit to the distribution with a standard deviation of 6 a.u.

4 Comparison of fragment momentum correlation for channels VI and VI*

It is explained in the main text that the fragmentation pathway that yields (CH_3^+ + $C_2H_3^+$), labeled channel VI*, follows the same general fragmentation mechanism as channel VI:

$$\begin{aligned} C_3H_7I^{2+} &\rightarrow CH_3^+ + C_2H_4I^+, \\ C_2H_4I^+ &\rightarrow C_2H_4^+ + I. \end{aligned} \tag{VI}$$

The fragment momentum correlation for these two channels for 1-IP, determined by two-fold covariance analysis, are compared in Figure S6. The signal-to-noise ratio is distinctly worse for the (CH_3^+, $C_2H_4^+$) ion pair but, otherwise, the distributions for both ion pairs match well. This confirms our assignment of the mechanism for channel VI*.

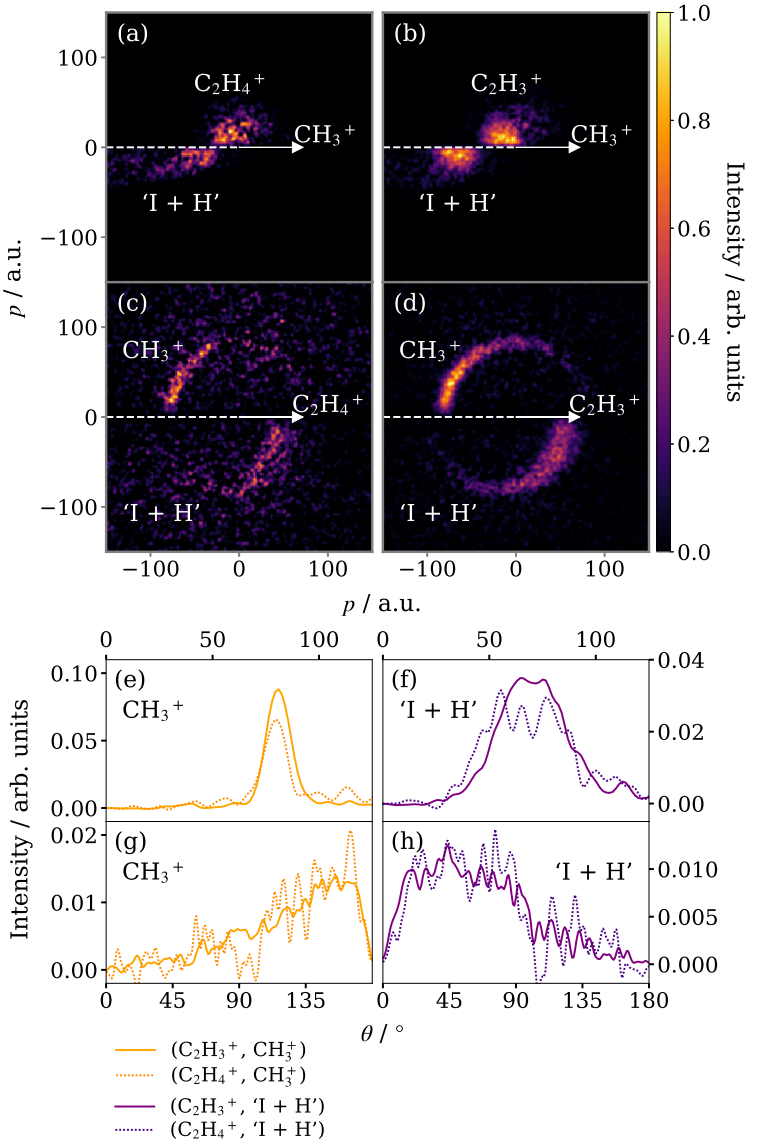

Figure S6: Newton diagrams for the sequential breakup of 1-IP^{2+} into CH_3^+ + $C_2H_4^+$ (*left column*, channel VI) and CH_3^+ + $C_2H_3^+$ (*right column*, channel VI*), involving Coulomb explosion into CH_3^+ + $C_2H_4I^+$ as the primary step. Panels (a, b) display the momentum distribution of $C_2H_x^+$ relative to the recoil direction of CH_3^+, and *vice-versa* in (c, d). Each panel is normalized separately. The momentum and angular distributions integrated from panels (c) and (d) and normalized to unit area are displayed below, indicated by dotted and solid lines, respectively.

5 Classical simulations of sequential three-body fragmentation dynamics

5.1 The effect of model parameters

Because the simulation does not consider a distribution of initial molecular geometries, the KER of the Coulomb explosion is fixed and, therefore, so are the momenta imparted to the fragments by this initial step. The key parameter that controls the output of the simulation is the impulse of the secondary dissociation p_s. This is demonstrated in Figure S7.

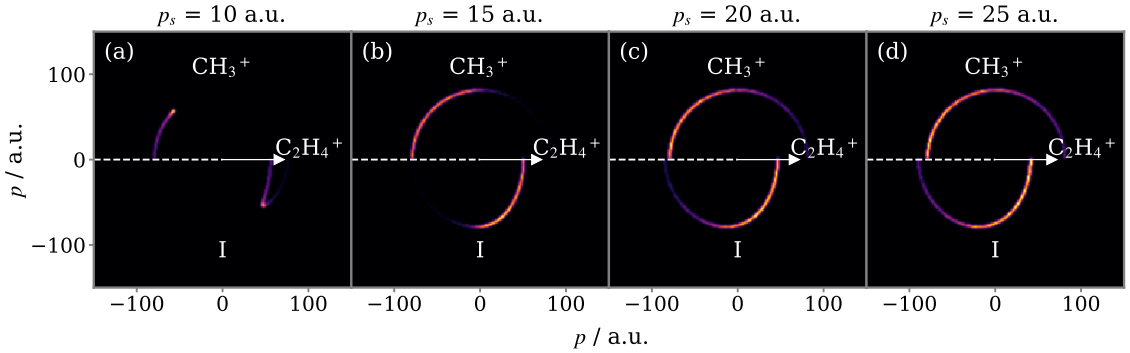

Figure S7: Simulated Newton diagrams for channel VI, the sequential three-body breakup of 1-IP^{2+} into ($CH_3^+ + C_2H_4^+ + I$), with $C_2H_4^+$ selected as the reference ion, showing how the output of the simulation varies as the secondary dissociation impulse (p_s) is changed.

If p_s was equal to zero, the ions would recoil back-to-back as the only influence on their trajectories would be the two-body Coulomb explosion. As p_s is increased, the angular span of the distribution stretches from 180° towards lower relative recoil angles. A greater p_s can more significantly perturb the trajectory of $C_2H_3^+$ relative to the recoil direction of CH_3^+. It is worth emphasizing that, whilst $C_2H_3I^+$ is randomly rotated in all of the simulations, only when p_s is large enough to exceed the momentum retained by $C_2H_3^+$ from the primary Coulomb explosion is the observed direction of travel of the $C_2H_3^+$ reversed by the secondary dissociation, generating ion pairs that recoil at an acute angle.

Incorporating a distribution of p_s is akin to summing several of the single-valued distributions shown here, generating features that have a width (see Figure S8(b) and (c)).

5.2 Simulation of channel VI* for 2-iodopropane

Figure S8 compares the experimental ($C_2H_3^+$, CH_3^+) covariance for 2-IP with simulated results. The parameters extracted from the experimental data and used as inputs for simulations include $p_s = 21 \pm 9$ a.u. and $\mathrm{KER}_p = 4.0 \pm 0.3$ eV, which equates to an effective separation of the charges on the CH_3^+ and $C_2H_4I^+$ moieties of 3.6 Å

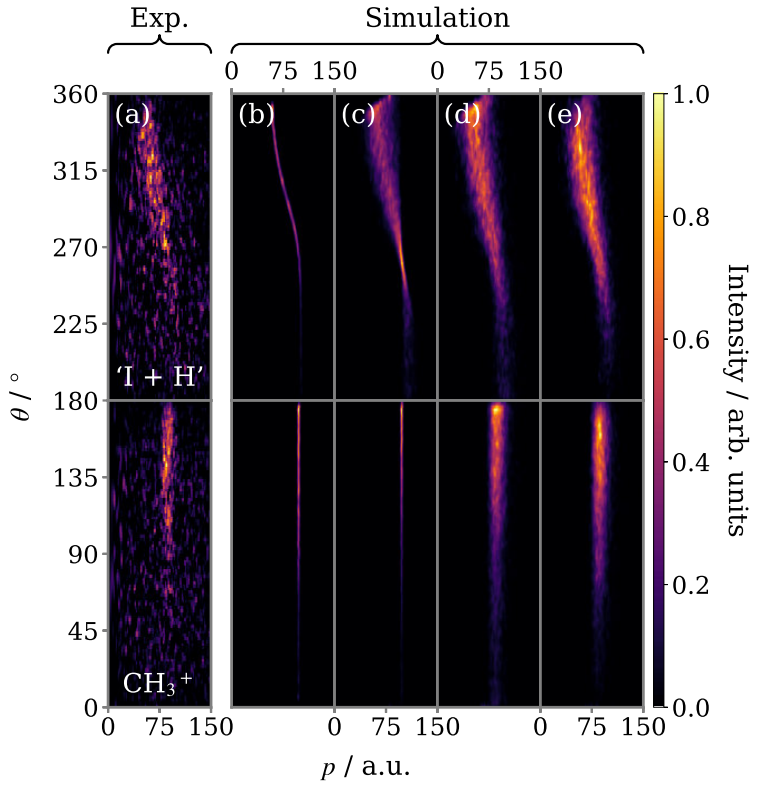

Figure S8: (a) The Newton diagram from Figure 6(d) displayed in polar coordinates, where θ is the angle relative to the recoil direction of CH_3^+. (b-e) Simulated covariance maps for channel VI*, the sequential breakup of 2-IP^{2+}, which yields CH_3^+ and $C_2H_3^+$ *via* a primary Coulomb explosion into $CH_3^+ + C_2H_4I^+$. (b) was produced by the model outlined in the methods section, (c) incorporates a distribution for the secondary-dissociation kinetic energy release, (d) uses an effective charge separation distribution for the primary step, and (e) also includes a small degree of out-of-plane rotation.

6 Additional covariance maps

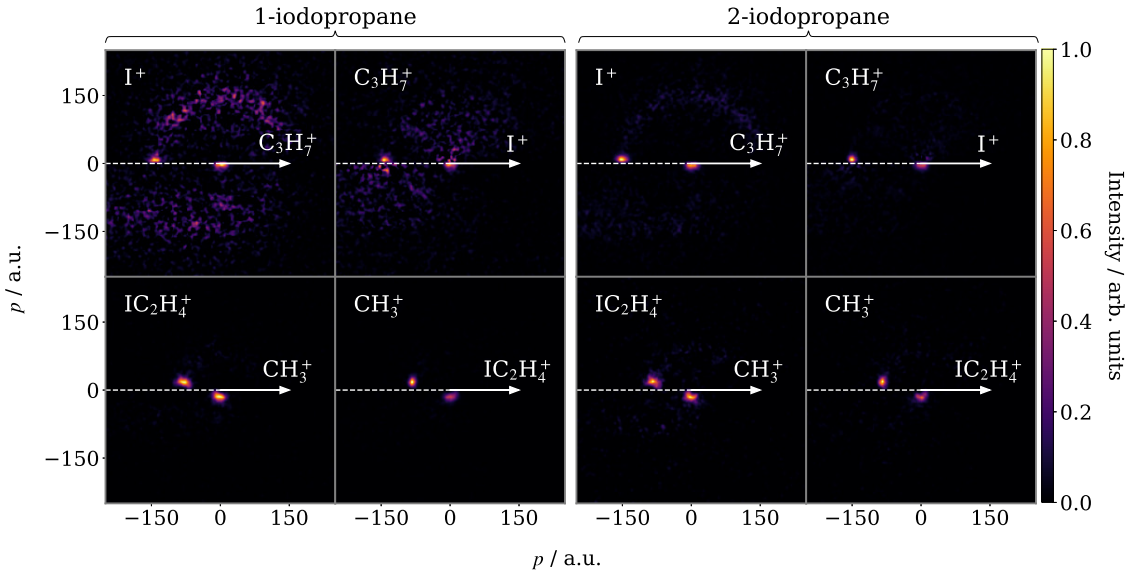

Figure S9: Newton diagrams for the two-body breakup of (*left*) 1-IP^{2+} and (*right*) 2-IP^{2+}

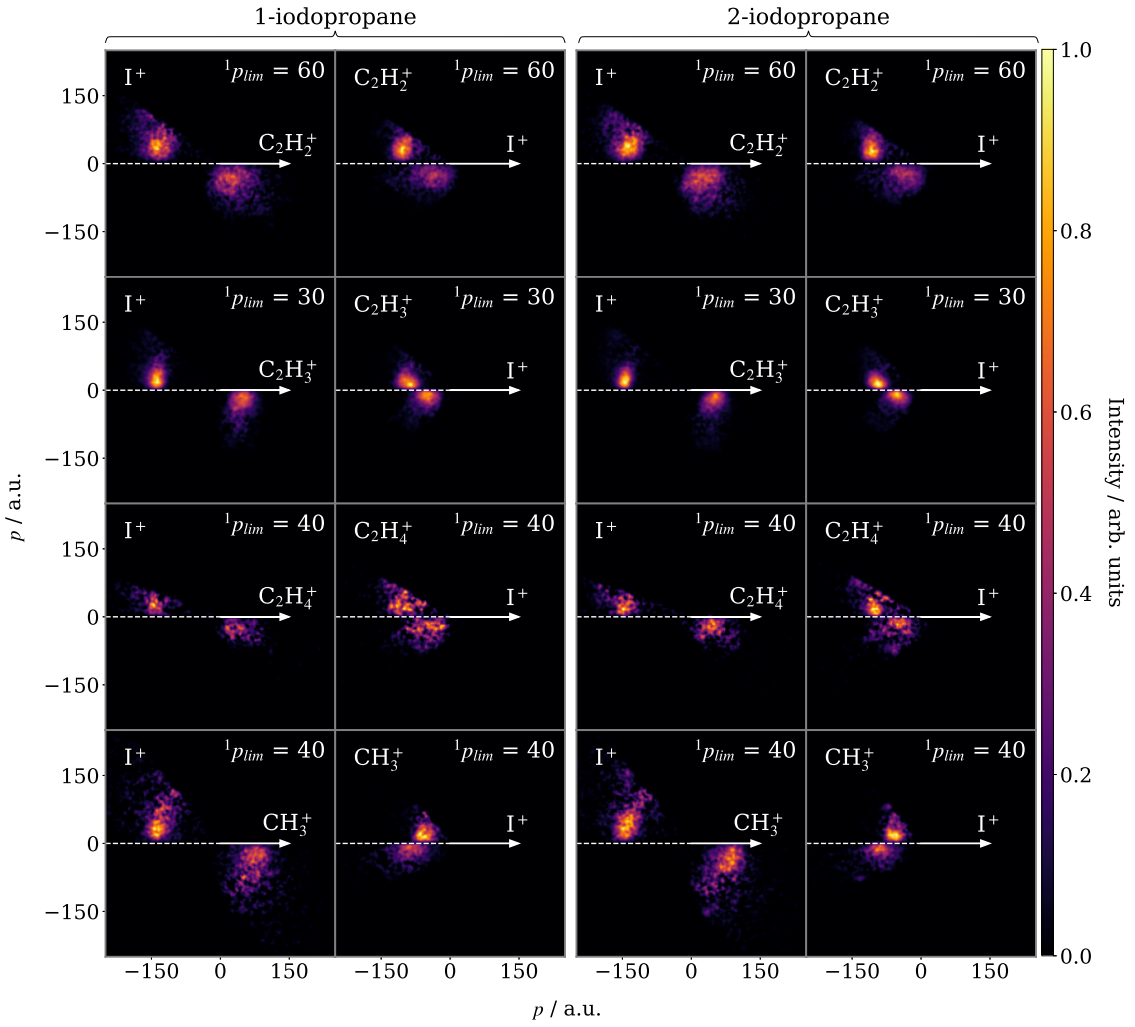

Figure S10: Newton diagrams for the sequential breakup of (*left*) 1-IP and (*right*) 2-IP involving Coulomb explosion into $I^+ + C_3H_7{}^+$ as the primary step. In the first and third columns, the primary ion product is the reference species, whilst in the second and fourth, the secondary ion product is the reference species. The ${}^1p_{lim}$ values used to isolate these features are given in each covariance map.

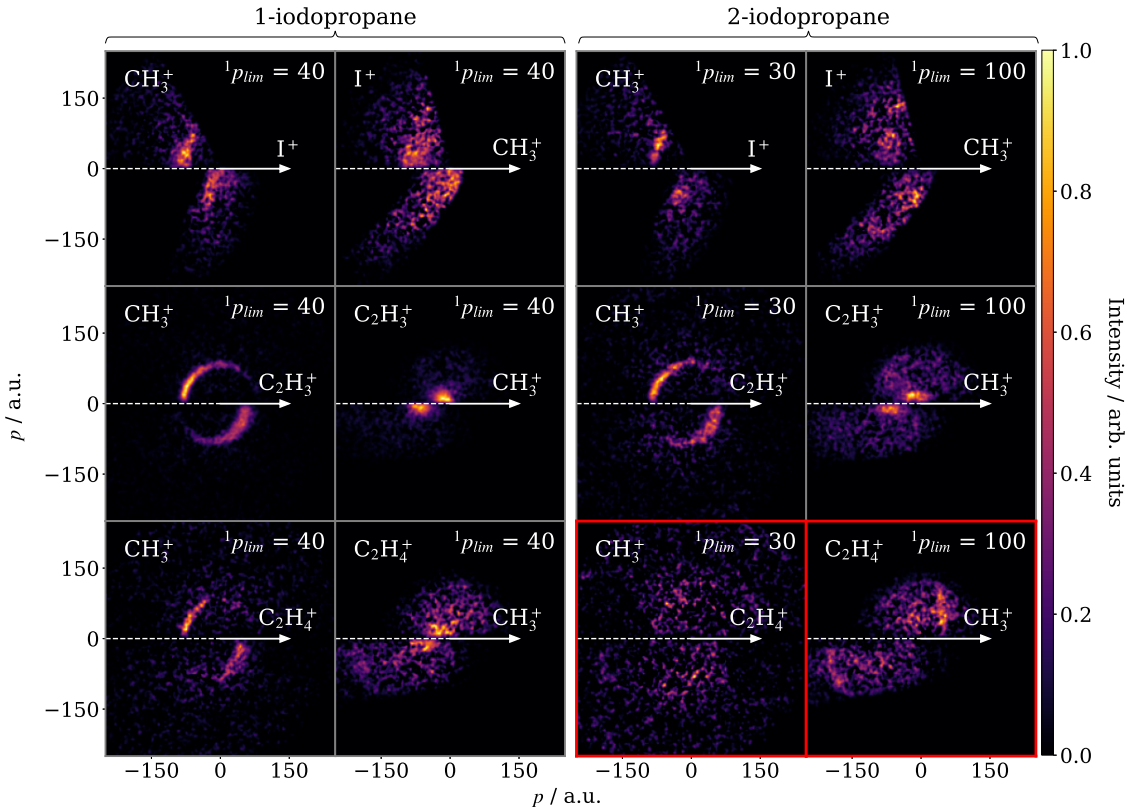

Figure S11: Newton diagrams for the sequential breakup of (*left*) 1-IP and (*right*) 2-IP involving Coulomb explosion into $CH_3^+ + C_2H_4I^+$ as the primary step. In the first and third columns, the primary ion product is the reference species, whilst in the second and fourth, the secondary ion product is the reference species. The ${}^1p_{lim}$ values used to isolate these features are given in each covariance map. Covariance maps that do not contain any discernible feature corresponding to this fragmentation channel are highlighted in red.